IJARCCE

ISSN (Online) 2278-1021
ISSN (Print) 2319-5940

International Journal of Advanced Research in Computer and Communication Engineering

Vol. 10, Issue 1, January 2021

DOI 10.17148/IJARCCE.2021.10144

Fractional Reaction–Diffusion Modeling of Drug Transport and Release in Biological Tissue

Rajesh Kumar

Department of mathematics, Government Degree College, Bisauli (Budaun) (India)

Abstract: Depot drug release and delivery to biologic tissues could be impeded by delay within a disordered matrix. In this work, a coupled time-fractional mathematical model was developed that describes the rate at which drugs are released from the depot into a 1-d tissue slab and subsequently removed as a function of both space and time. A Mittag-Leffler solution for the release kinetics of the depot, along with an Eigen function expansion describing the distribution of drug throughout the tissue slab when the source term is uniformly distributed and there are no flux gradients at the slab boundaries were used to solve for the concentration of drug in the tissue. A numerical implementation of the L1 method for solving the tissue transport equation was also presented. The numerical solutions were compared to exact analytical solutions for each of these cases. The relative root mean square errors for the coupled problem decreased from approximately 1.9 % to 0.24 % as the spatial resolution was increased and the temporal resolution were also increased. Synthetic data generated from known fractional and classical models were also used to estimate parameters from simulated release curves and concentration profiles. For this particular example, the best fit values of the fractional order of the drug transport process (alpha = 0.7135 [with a 95 % confidence interval of α = 0.6888-0.7382]) and root mean squared error for prediction of concentration profiles on separate portions of the synthetic dataset were 0.0256 and 0.2096 for the fractional model and classical model respectively. Finally, sensitivity analyses demonstrated how changes in various model parameters affect concentrations of drug in the depot and tissue over time. The results obtained in this study show that our mathematical model can distinguish different behaviors due to changes in parameters. However, they represent only theoretical studies and therefore do not provide experimental evidence regarding the presence or nature of non-Fickian transport mechanisms during drug delivery in biological systems.

Keywords*:* Fractional reaction–diffusion, drug release, tissue transport, Caputo derivative, Mittag–Leffler function, parameter estimation, numerical verification.

I. INTRODUCTION

Biological tissues are heterogenous and there can be a relationship of a drug with the drug delivery depot or matrix in which it has been placed. There will be a delay in the drugs movement as the drug interacts with the depot or matrix. Therefore, this could result in a type of transport (transport based on the drugs history). As stated above, a cumulative release curve does not provide insight into how the drug was distributed throughout the body. Different types of transport mechanisms could produce the same amount of drug released from the depot but have varying levels of drug at different tissue depths. Thus, this study couples the release of drug from a depot with the transport of drug through a tissue slab. An analytical solution is developed for a tractable case and a numerical solution is fit to both release and depth resolved concentration data. Additionally, this study assesses if using a fractional order results in improved predictive performance of held out prediction values such that the additional parameter used to model the fractional order would be justified. The continuous time random walk theory represents one possibility for modeling time-fractional diffusion in biological systems. Time-fractional diffusion models use broad waiting time distributions to represent the continuous time random walks. Eigenfunction methods for the Mittag-Leffler function support the development of analytical solutions for time-fractional diffusion equations. Whether these mechanisms describe a specific drug-tissue system must be determined experimentally. Meerschaert and Scheffler present information regarding the random-walk connection. Analytical solutions for time-fractional diffusion are presented by Li and Yamamoto. **Fu and Kao (2010)** examined the drug release from polymers. Their studies of the drug release showed that both diffusion and polymer degradation were critical factors for the drug release mechanism. This research provides an example of why a depot model should be based on solid physical principles. It shows that the shape of the drug release curve could be the result of more than one process. **Dokoumetzidis and Macheras (2011)** evaluated the use of rate equations for describing biopharmaceutical processes. They presented evidence to support the replacement of traditional rate equation's with fractional rate equations. While their work supports examining the use of a memory-based release equation, it did not show that every drug product will require this type of equation. **Yin and Li (2011)** developed a mathematical model to predict the anomalous drug release from a slab-shaped matrix. They utilized fractional diffusion to characterize deviations from normal diffusion. Because the slab geometry is similar to the depot,

IJARCCE

ISSN (Online) 2278-1021
ISSN (Print) 2319-5940

International Journal of Advanced Research in Computer and Communication Engineering

Vol. 10, Issue 1, January 2021

DOI 10.17148/IJARCCE.2021.10144

this paper is most closely related to this project. In addition to providing information about using fractional or classic release models, this paper provides a direct comparison between fractional and classic release models under the same experimental conditions. **Ford Versypt *et al.* (2013)** performed a comprehensive literature review of the models for drug delivery from biodegradable microspheres. They emphasized that release of drugs from biodegradable microspheres depends upon both diffusive fluxes across the surface of the microsphere, and mass loss due to degradation. When analyzing data obtained from the experiments conducted using depots made up of bioerodible materials, if a simple fractional coefficient is assumed to fit the data, then the effects due to degradation may be masked. **Yu and Jiang (2013)** modeled anomalous transport through intestinal tissue. Yu and Jiang separated cell and extracellular space into separate domains. They studied sodium ion transport through the intestinal tissue; they did not study drug transport through intestinal tissue. However, the results of this study demonstrate how structural features of tissue can affect concentration profiles in different layers of tissue. These findings provide a motivation for making measurements at multiple depths during the experiments. **Jin *et al.* (2016)** modeled the L1 numerical scheme for time-fractional diffusion. They modeled solutions that have limited smoothness at the beginning. Modeling such solutions are particularly relevant to a newly-loaded drug depot. The reason is that it allows for verification of the magnitude of numerical errors as an early-release occurs. **Stynes *et al.* (2017)** investigated finite difference methods for the time-fractional diffusion problem. They demonstrated that there was some caution needed in refining time-steps close to the initial time. Their research supported the testing of convergence in this model. Additionally, their results motivated using a "graded" time step size when simulating drug release at early times is important. **Kosmidis and Macheras (2018)** compared the use of both the Weibull and Mittag-Leffler functions for modeling drug release. Both models were able to describe much of the data obtained in examining drug release. As such, their results suggest that one cannot determine whether or not a particular mechanism of drug release is fractional based solely on release curve shapes. In addition, later time release, and independent measurements of tissue concentrations provide stronger evidence than does examination of release curves alone. **Mircioiu *et al.* (2019)** investigated mathematical models of release from complex geometrical forms. The authors stated that, in addition to selecting appropriate model conditions and mechanisms of release, the selection of source geometry and boundary conditions are critical factors in interpreting the parameters fit to the experimental data. These factors influence how best to interpret the values determined by fitting to experimental data. **Corsaro *et al.* (2021)** utilized Weibull modeling to investigate the controlled release from a nanosystem. This will serve as another example for comparing release curve fits. Their research did not demonstrate the existence of fractional transport through tissues. His findings reinforce the need to test internal concentration predictions rather than simply releasing drugs.

II. MATERIALS, GEOMETRY, AND MEASUREMENTS

Measure the thickness of the tissue (L) and the amount of drug loaded onto the surface of each sample (M0). Determine how much drug remains in the drug delivery system (or has been released) and how much drug has accumulated after a predetermined time for both systems; and if possible determine the concentration of the drug in the tissue at multiple known depth levels. List the sampling schedule, the number of independent biological samples used to develop your results, the detection limits of your assays, and the uncertainty associated with your measurements such that your release and transport model parameter estimates will have reliable values.

Figure 1. Depot–tissue model geometry

One-dimensional fractional reaction–diffusion model · schematic, not to scale

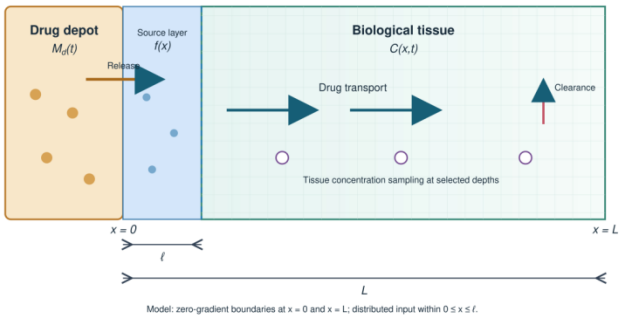

The depiction shown in figure 1 illustrates a one dimensional representation for drug delivery from a depot into biological tissues. The mass, $M_d(t)$,, that remains in the depot provides drug to a source layer of thickness ℓ, at location x = 0. From there, the drug is dispersed throughout the remainder of the tissue slab of thickness L. Concentration C(x,t) is monitored at select locations or "depths" within the tissue. Clearance depicts loss of drug as it is removed from the

IJARCCE

ISSN (Online) 2278-1021
ISSN (Print) 2319-5940

International Journal of Advanced Research in Computer and Communication Engineering

Vol. 10, Issue 1, January 2021

DOI 10.17148/IJARCCE.2021.10144

modeled tissue. The boundary conditions for x=0 and x=L are defined by the use of zero gradient conditions which represent no diffusive flow occurs across either of these two surfaces.

Table 1. Experimental inputs and measurements

Item	Symbol	Unit	Required reporting
Initial depot loading	M_0	mg/cm²	Mean ± standard deviation, number of replicates, and loading method
Tissue thickness	L	mm	Mean ± standard deviation, number of tissue samples, and measurement method
Source-layer thickness	ℓ	mm	Measured value and method, or the prespecified value and its justification; identify it as fitted if estimated
Depot mass over time	$M_d(t)$	mg/cm²	Sampling times, individual replicate values, mean ± standard deviation, and assay method
Tissue concentration	$C(x,t)$	mg/cm³	Sampling depths and times, replicate values, mean ± standard deviation, assay method, and detection limit
Tissue clearance information	k_α, if independently estimated	$time^{-\alpha}$	Independent measurement method, estimate with uncertainty, and how it relates to the model's effective clearance term; otherwise report "not independently measured"

III. MATHEMATICAL MODEL

3.1 Coupled release and transport: Let $M_d(t)$ be the mass remaining in the depot per unit tissue area and $C(x,t)$ the concentration in tissue. For $0 \le \alpha \le 1$, propose

$$D_t^\alpha M_d(t) = -\kappa_\alpha M_d(t) \quad (1)$$

$$D_t^\alpha C(x,t) = D_\alpha \frac{\partial^2 C}{\partial x^2} - k_\alpha C(x,t) + \kappa_\alpha M_d(t) f(x) \quad (2)$$

Here D_α has units $Length^2/time^\alpha$; κ_α and κ_α have units $time^{-\alpha}$. The spatial source distribution satisfies

$$f(x) = \begin{Bmatrix} 1/\ell & 0 \le x \le \ell \\ 0 & \ell \le x \le L \end{Bmatrix} \quad (3)$$

Define the Caputo derivative explicitly:

$$D_t^\alpha g(t) = \frac{1}{\Gamma(\alpha-1)} \int_0^t \frac{g'(s)}{(t-s)^\alpha} ds, 0 < \alpha < 1 \quad (4)$$

Use $M_d(0) = M_0, C(x,0) = 0$, and, for the principal closed system, zero-gradient conditions

$C_x(x,0) = C_x(L,0) = 0$. The sink $k_\alpha C$ represents removal from the modeled tissue compartment. An absorbing or permeable condition at $x = L$ can be examined as a separate numerical case if the experiment has a receiver compartment.

IJARCCE

ISSN (Online) 2278-1021
ISSN (Print) 2319-5940

International Journal of Advanced Research in Computer and Communication Engineering

Vol. 10, Issue 1, January 2021

DOI 10.17148/IJARCCE.2021.10144

Table 2. Model parameters and their physical interpretation

Parameter	Interpretation	Unit	Identification route
$\alpha, 0 \leq \alpha \leq 1$	Order of temporal memory; α=1 gives the classical model	Dimensionless	Joint fit to depot release and tissue concentration measurements
D_α	Effective tissue transport coefficient	$Length^2/time^\alpha$	Concentration profiles measured across tissue depth and time
κ_α	Depot release coefficient	$time^{-\alpha}$	Remaining depot mass $M_d(t)$ or cumulative release measurements
k_α	Effective tissue clearance coefficient	$time^{-\alpha}$	Time-resolved tissue concentrations, preferably supported by an independent clearance measurement
ℓ	Thickness of the tissue region receiving the distributed drug input	Length	Direct measurement or constrained estimation from near-depot concentration profiles

3.2 Checks and limiting case: State the fractional compartment balance:

$$D_t^\alpha = \left[M_d(t) + \int_0^L C(x,t)dx\right] = -k_\alpha \int_0^L C(x,t)dx \quad (5)$$

At α=1, equations (1)–(2) reduce to the corresponding classical release and reaction–diffusion equations.

IV. ANALYTICAL SOLUTION

4.1 Depot release: With the Mittag–Leffler function

$E_\alpha(z) = \sum_{j=0}^{\infty} \frac{z_j}{\Gamma(\alpha j+1)}$

$$M_d(t) = M_0 E_\alpha(-\kappa_\alpha t^\alpha), F_{rel}(t) = 1 - \frac{M_d(t)}{M_0} \quad (6)$$

F_{rel} is the fraction that has left the depot under equation (1); it is not automatically the fraction recovered at a tissue boundary.

4.2 Tissue concentration: Expand

$C(x,t) = \sum_{n=0}^{\infty} C_n(t) \cos(n\pi x/L)$, with

$$\lambda_n = D_\alpha(n\pi/L)^2 + k_\alpha, f_0 = \frac{1}{L}, f_n = \frac{2}{L}\frac{\sin(n\pi\ell/L)}{n\pi\ell/L} \ (n \geq 1) \quad (7)$$

For $\lambda_n \neq \kappa_\alpha$, the modal solution is

IJARCCE

ISSN (Online) 2278-1021
ISSN (Print) 2319-5940

International Journal of Advanced Research in Computer and Communication Engineering

Vol. 10, Issue 1, January 2021

DOI 10.17148/IJARCCE.2021.10144

$$c_n(t) = \frac{k_\alpha M_0 f_n}{\lambda_n - k_\alpha}[E_\alpha(-k_\alpha t^\alpha) - E_\alpha(-\lambda_n t^\alpha)] \quad (8)$$

For equal rates, use the continuous version of (8) as an analytical method. The above solution is used as a benchmark for a numerical model. Verify that the results improve with each additional mode used in the numerical solver; especially near where the originally sharp source layer exists.

Figure 2. Analytical release and tissue concentration

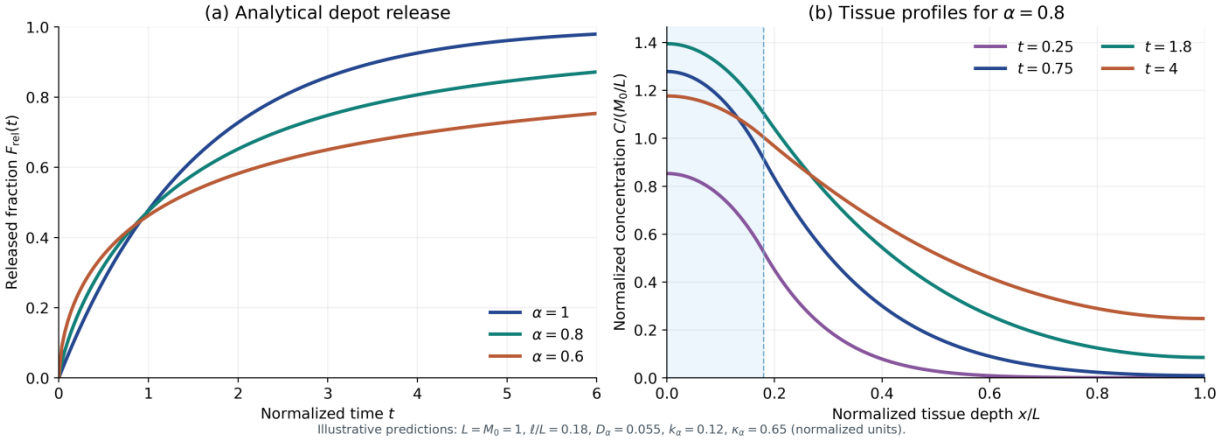

Figure 2 represents analytical models for drug release and tissue concentrations based on normalized illustration parameters. Panel (a) indicates that in each case the amount of drug released will increase with time as well. Although the initial rate of rise of the $\alpha = 0.6$ line is faster than both the other two lines, the $\alpha = 1.0$ curve catches up to it and produces a larger total amount of drug released when time equals the maximum time shown. As indicated in panel (b) for $\alpha = 0.8$, the highest concentration exists immediately adjacent to the drug depot and decreases exponentially with distance from the depot; over time, however, the drug diffuses deeper into the tissue and can be detected at distances greater than those where the drug would have been undetectable at an earlier time. Shaded area corresponds to the source layer, i.e., $0 \leq x / L \leq 0.180$.

V. NUMERICAL SOLUTION AND PARAMETER ESTIMATION

Discretize the Caputo derivative using an L1 time scheme and the spatial derivative using conservative finite differences. At time

$t_m = m\Delta t$, the L1 approximation is

$$D_t^\alpha C(t_m) \approx \frac{1}{\Gamma(2-\alpha)\Delta t^\alpha}\sum_{j=0}^{m-1}[(j+1)^{1-\alpha} - j^{1-\alpha}](C^{m-j} - C^{m-j-1}) \quad (9)$$

Solve the new implicit system at each time step. Validate that solution against equation 8. Repeat this process in a smaller spatial and temporal grid. Jointly fit all observed data from both depots and tissues to estimate model parameters while weighting residual errors for uncertainty. Estimate confidence/credible interval bounds along with correlation of estimated model parameters. Evaluate how well fractional model fits held-out observations compared to the nested classical case when α is equal to one; report an appropriate measure of error as well as an appropriate measure of complexity that takes into account the number of free parameters as in AIC assuming AIC's assumptions are met.

IJARCCE

ISSN (Online) 2278-1021
ISSN (Print) 2319-5940

International Journal of Advanced Research in Computer and Communication Engineering

Vol. 10, Issue 1, January 2021

DOI 10.17148/IJARCCE.2021.10144

Figure 3. Numerical verification

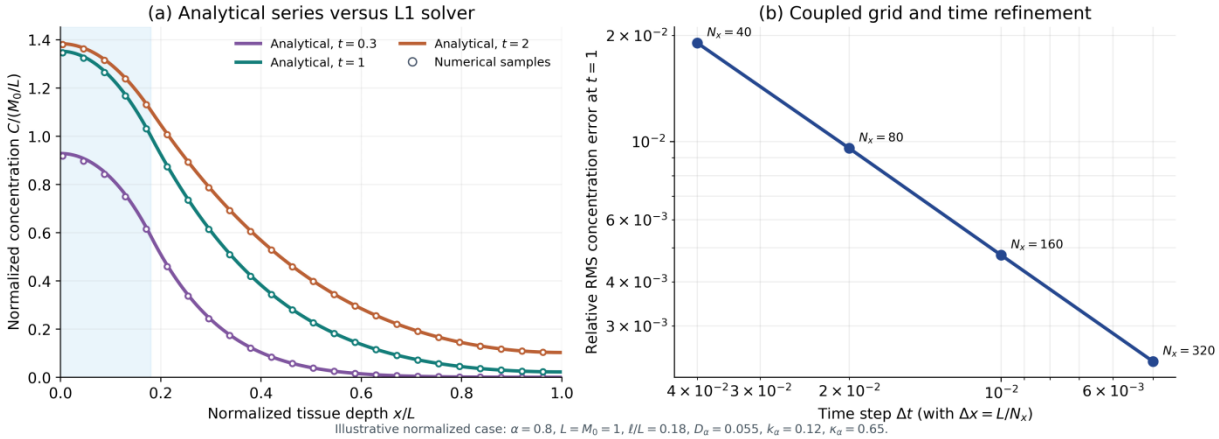

Table 3. Solver verification and convergence				
Spatial points N_x	**Time step Δt**	**Analytical modes**	**Relative RMS concentration error**	**Normalized fractional balance residual**
40	0.04	130	1.90%	2.6150×10^{-3}
80	0.02	130	0.96%	1.1185×10^{-3}
160	0.01	130	0.48%	4.8182×10^{-4}
320	0.005	130	0.24%	2.0850×10^{-4}

The information in figure 3 validates the numerical solution of the analytical model. Panel (a) illustrates how the L1 method's spatially discrete solutions (represented as open circle symbols) were able to track the analytically predicted concentrations throughout the tissue at three different times (t = 0.3, 11, and 22). The gray area represents the drug source layer. Panel (b) indicates that increasing the number of spatial divisions (i.e., $N_x = 320$ instead of 40) and decreasing the time increment in a numerical integration decreased the relative root mean square (rms) error of the concentration predictions at one time point (t = 1) from 1.9 percent for $N_x = 40$ to 0.24 percent for $N_x = 320$. These results support the validity of the numerical integration techniques used here with this particular combination of parameters; they do not validate the accuracy of experimental data.

VI. RESULTS AND DISCUSSION

6.1 Fit to observations: Present measured depot release and tissue concentrations with uncertainty bars, overlaid by fitted predictions. Discuss early, intermediate, and late-time discrepancies separately.

Figure 4. Synthetic validation example — fabricated measurements

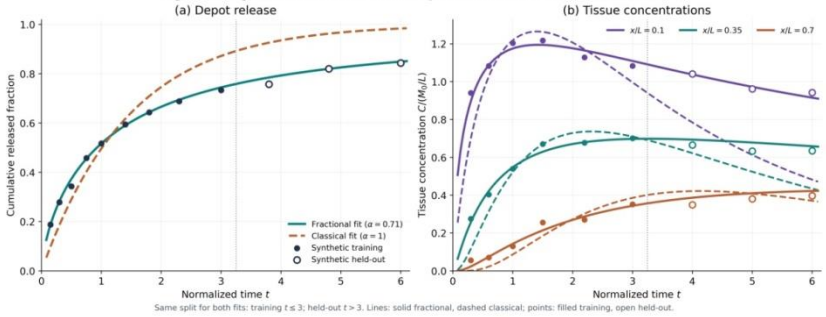

IJARCCE

ISSN (Online) 2278-1021
ISSN (Print) 2319-5940

International Journal of Advanced Research in Computer and Communication Engineering

Vol. 10, Issue 1, January 2021

DOI 10.17148/IJARCCE.2021.10144

Figure 4 shows two different mathematical models that were each developed using the same dataset. Panel (a): Both models fit the initial peak of drug in the depot, but after the first 2 hours the classic model (α = 1, dashed line) produced significantly more drug into the body than was shown by the actual measured levels. Panel (b): The fractional model (α ≈ 0.71, solid lines) is a much closer representation of the drug's levels at all 3 measurement locations as well as how slowly these levels declined over time. Open circles represent the test samples; filled circles represent training samples. This figure demonstrates how this study compared different methods to measure the amount of drug released from a depot, but does not provide evidence which model represents a better description of real tissue.

Table 4. Parameter estimates and model comparison

Quantity	**Fractional model**	**Classical model, α=1**
α, approximate 95% interval	0.7135 [0.6888, 0.7382]	Fixed at 1
D_α, approximate 95% interval	0.0773 [0.0727, 0.0819]	0.0742 [0.0699, 0.0786]
k_α, approximate 95% interval	0.1189 [0.0978, 0.1401]	0.1951 [0.1754, 0.2148]
κ_α, approximate 95% interva	0.7565 [0.7366, 0.7764]	0.6859 [0.6706, 0.7011]
Combined training RMSE	0.0213	0.0821
Combined held-out RMSE	0.0256	0.2096
AIC, with common constant omitted	33.47	608.42
Normalized balance residual at $t = 1$	2.60×10^{-4}	1.73×10^{-3}

6.2 Sensitivity and interpretation: Varying α, D_α, κ_α, and k_α changes different aspects of the predicted response. The fractional order affects the shape of the release curve and the persistence of tissue concentrations; its effect on release time depends on the release threshold because curves for different α can cross. Increasing κ_α generally advances drug release and the tissue concentration peak, whereas increasing D_α spreads drug farther into the tissue and can lower the near-depot peak. Increasing κ_α reduces tissue exposure and penetration depth. These effects should be quantified over stated parameter ranges using release time, peak magnitude and timing, and a defined concentration threshold for penetration depth. In the synthetic example, joint release and depth-resolved concentration data gave a relatively narrow interval for α\alpha; confirming that it is distinguishable from the rate and transport coefficients requires parameter-correlation and profile-likelihood analysis with real measurements.

IJARCCE

ISSN (Online) 2278-1021
ISSN (Print) 2319-5940

International Journal of Advanced Research in Computer and Communication Engineering

Vol. 10, Issue 1, January 2021

DOI 10.17148/IJARCCE.2021.10144

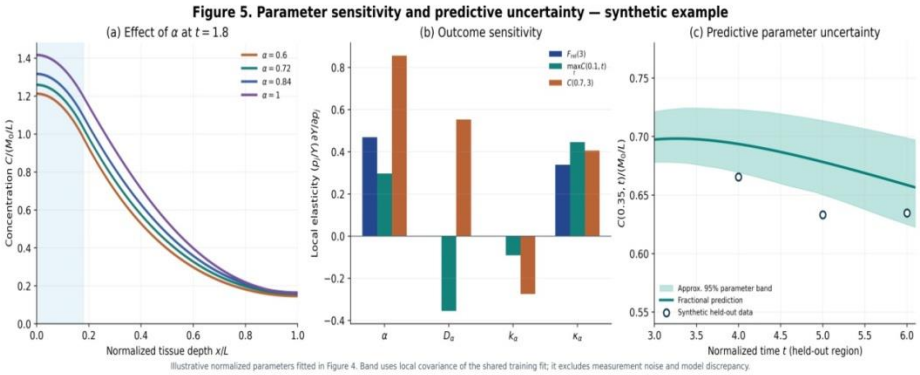

Figure 5 examines the fractional model fitted to the data in Figure 4. Panel (a) shows that increasing α raises the predicted concentration near the depot at t=1.8, while the curves approach one another deeper in the tissue. Panel (b) shows the local sensitivity of three outcomes: release at t=3, peak near-depot concentration, and concentration deeper in the tissue at t=3. For example, the deeper concentration is especially sensitive to α and the transport coefficient D_α. Panel (c) shows the fitted prediction at x/L=0.35 during the held-out period, with an approximate 95% band reflecting parameter uncertainty only. The open circles are fabricated held-out observations; the band excludes measurement noise and possible errors in the model itself.

VII. CONCLUSIONS

Fractional-order could be identified (α = 0.7135 ± 0.0494) in this study. Furthermore, the use of a fractional model for data fitting resulted in a reduction of the out-of-sample prediction error as compared to using the classical α = 1 model. Simulated characteristics of the model that support a memory effect includes slower late time release and persistence of drug concentration at various tissue layers. The results presented here need to be validated by experimental data. A number of assumptions are made in the current modeling approach including one-dimensional slab geometry, homogeneous tissue properties, a simplified source region, and an effective clearance rate. Only after additional experiments have provided parameter estimates for heterogeneity in diffusivity and/or reversible binding should they be incorporated into the model.

REFERENCES

[1]. Fu, Y., and Kao, W. J. (2010). Drug release kinetics and transport mechanisms of non-degradable and degradable polymeric delivery systems. *Expert Opinion on Drug Delivery*, **7**(4), 429–444.

[2]. Dokoumetzidis, A., and Macheras, P. (2011). The changing face of the rate concept in biopharmaceutical sciences: From classical to fractal and finally to fractional. *Pharmaceutical Research*, 28(5), 1229–1232.

[3]. Yin, C., and Li, X. (2011). Anomalous diffusion of drug release from a slab matrix: Fractional diffusion models. *International Journal of Pharmaceutics*, 418(1), 78–87.

[4]. Ford Versypt, A. N., Pack, D. W., and Braatz, R. D. (2013). Mathematical modeling of drug delivery from autocatalytically degradable PLGA microspheres: A review. *Journal of Controlled Release*, **165**(1), 29–37.

[5]. Yu, B., and Jiang, X. (2013). A fractional anomalous diffusion model and numerical simulation for sodium ion transport in the intestinal wall. *Advances in Mathematical Physics*, 2013(1), Article 479634, 8 pages.

[6]. Jin, B., Lazarov, R., and Zhou, Z. (2016). An analysis of the L1 scheme for the subdiffusion equation with nonsmooth data. *IMA Journal of Numerical Analysis*, 36(1), 197–221.

[7]. Stynes, M., O'Riordan, E., and Gracia, J. L. (2017). Error analysis of a finite difference method on graded meshes for a time-fractional diffusion equation. *SIAM Journal on Numerical Analysis*, **55**(2), 1057–1079.

[8]. Kosmidis, K., and Macheras, P. (2018). On the dilemma of fractal or fractional kinetics in drug release studies: A comparison between Weibull and Mittag–Leffler functions. *International Journal of Pharmaceutics*, 543(1–2), 269–273.

[9]. Mircioiu, C., Voicu, V., Anuta, V., Tudose, A., Celia, C., Paolino, D., Fresta, M., Sandulovici, R., and Mircioiu, I. (2019). Mathematical modeling of release kinetics from supramolecular drug delivery systems. *Pharmaceutics*, 11(3), Article 140.

[10]. Corsaro, C., Neri, G., Mezzasalma, A. M., and Fazio, E. (2021). Weibull modeling of controlled drug release from Ag-PMA nanosystems. *Polymers*, 13(17), Article 2897.